Effect of carbon nanotube buckypapers on interlaminar fracture toughness of thermoplastic composites subjected to fatigue tests

de Paula Santos, Luis Felipe; Monticeli, Francisco Maciel; Ribeiro, Bruno; Costa, Michelle Leali; Alderliesten, René; Botelho, Edson Cocchieri

DOI
10.1016/j.ijfatigue.2025.108868

Publication date
2025

Document Version
Final published version

Published in
International Journal of Fatigue

International Journal of Fatigue 195 (2025) 108868

Contents lists available at ScienceDirect

International Journal of Fatigue

journal homepage: www.elsevier.com/locate/ijfatigue

Effect of carbon nanotube buckypapers on interlaminar fracture toughness of thermoplastic composites subjected to fatigue tests

Luis Felipe de Paula Santos [a,b,*], Francisco Maciel Monticeli [c], Bruno Ribeiro [d], Michelle Leali Costa [a,e], René Alderliesten [c], Edson Cocchieri Botelho [a]

[a] São Paulo State University (UNESP) School of Engineering and Science Department of Materials and Technology Guaratinguetá Brazil
[b] Institute for Technological Research (IPT) Lightweight Structures Laboratory São José Dos Campos Brazil
[c] Delft University of Technology (TU-Delft) Aerospace Engineering Structural Integrity & Composites Delft Netherlands
[d] Federal University of Sao Paulo (UNIFESP) Institute of Science and Technology São José Dos Campos Brazil
[e] Ganesha Institute of Innovation Science and Technology São José Dos Campos Brazil

ARTICLE INFO

Keywords:
Fatigue behavior
Interlaminar fracture toughness
Thermoplastic composites
Buckypapers
Fractography

ABSTRACT

Three-phase composites, especially those composed of high performance thermoplastics, have not been properly investigated with respect to their interlaminar fracture toughness. Therefore, this study investigates effect on the interlaminar fracture toughness by adding carbon nanotube buckypaper (BP), tested under cyclic loading in mode I and II. BP weakened the interlaminar fracture toughness in mode I, creating an easy path for crack growth and reducing the strain energy release (SERR) values in the Paris curves. Conversely, under mode II BPs presented no significant influence to the interlaminar fracture toughness and fatigue life; however, a slight improvement was observed due to the bridging effect. The energy balance principle model for opening delamination showed that BP composites require less energy per unit of area to crack growth, resulting in a smoother fracture surface with fewer failure mechanisms. In contrast, BP slightly increased the energy per unit of area for crack growth, leading to a rougher fracture surface with a higher prevalence of failure mechanisms under mode II. This work underscores the importance of examining the individual effects of mode I and II loadings on BP laminates since these interleaves affect the interlaminar toughness and fatigue life differently.

1. Introduction

The requirements for advanced materials have been widely explored in various industrial sectors, particularly those focused on lightweight structures. Carbon fiber-reinforced polymer composites (CFRPs), particularly those with a high-performance thermoplastic matrix, have achieved significant progress in terms of design optimization, weight reduction, and structural integrity [1–3]. Thermoplastic composites are particularly attractive to the industry due to their properties, including high fracture toughness, impact resistance, increased stiffness and specific strength, chemical and environmental resistance, recyclability, and the ability to be joined by welding techniques, these properties compared to thermoset composites [4]. These properties make them attractive to some industries such as aerospace and aeronautical [5].

Nevertheless, CFRPs laminates are characterized by lower interlaminar strength, rendering them susceptible to delamination throughout their service life [6–8]. Delamination is an interlaminar failure that often appears as a primary failure mode, occurring between two plies within the laminate due to interlaminar stresses acting at the interface. This type of failure is categorized as mode I (opening), mode II (shear), mode III (tearing), and mixed mode, generally related to the opening modes [9]. Mode I involve open delamination due to the normal tensile stress through the thickness, promoting debonding at the interface. On the other hand, modes II and III are associated with the in-plane and out-of-plane shear stress, respectively, that induces sliding between the layers (upper and lower). The mixed mode combines elements of the aforementioned failure modes [10].

In addition to interlaminar failure, fatigue is the predominant cause of failure in structural composite components. Therefore, comprehensively understanding the interlaminar properties under dynamic loading conditions is imperative for accurately estimating the service life of CFRPs. Within this context, several researchers have investigated delamination growth in CFRPs under cyclic loading [11–13], but only a limited number of papers focus on delamination growth in thermoplastic composites, particularly those reinforced with nanoparticles. Amaral et al. [14] suggest that several similitude parameters can be used to

* Corresponding author.

https://doi.org/10.1016/j.ijfatigue.2025.108868
Received 25 October 2024; Received in revised form 14 January 2025; Accepted 7 February 2025
Available online 8 February 2025

estimate fatigue delamination curves. Some authors use G_{max} (the maximum Strain Energy Release Rate – SERR), it represents the maximum stored elastic energy available for crack propagation during one cycle. While, others apply the standard Paris parameter range ($\Delta G = G_{max} - G_{min}$), which is analogous to stress intensity factor formulation (ΔK) accounts for the cyclic nature of loading and the contribution of both the maximum and minimum values to the fatigue crack growth. The use of $\Delta\sqrt{G}$ (square root of energy release rate range) used to linearize the relationship between the energy release rate and crack growth and highlight the difference of stress ratio, is more closely related to ΔK, since $K \propto \sqrt{G}$. Additionally, the actual SERR is determined by measuring specific data during the fatigue test, such as crack length (a), displacement (δ), force (P), and number cycles (N), enabling plotting a graph of da/dN versus dU/dN. Furthermore, dU/dA is also obtained through the inverse of the slope of the curve as a function of the inverse of the sample width [14]. Also, the rate of change of dissipated energy (dU/dt) could be plotted against the crack tip propagation speed (da/dt). In this case, dU/dA or $\frac{1}{b}\frac{dU/dt}{da/dt}$ relate to the mean SERR value rather than $\Delta\sqrt{G}$ or ΔG. This similitude parameter is based on the energy balance and can be applied to analyze quasi-static delamination data. This approach facilitates a comparison between fatigue and quasi-static loading, helping to identify the differences in energy release [15].

$$G^{*} = \frac{1}{b}\frac{dU/dN}{da/dN} = \frac{1}{b}\frac{dU/dt}{da/dt} \tag{1}$$

Among the available methods, the incorporation of carbonaceous nanoparticles within the matrix [16], in-situ fiber growth/grafting [17], and the use of interlayers as macroscopic assemblies (such as nanoparticle films, including carbon nanotube buckypaper or graphene papers) are particularly noteworthy [4]. These methods not only enhance mechanical properties but also introduce multifunctional characteristics to the composite material — such as thermal, electrical, or optical properties — that contribute to the overall optimization of the system [18].

The effectiveness of CNT incorporation has been reported in various studies. He et al. [17] incorporated 0.3 wt% of CNT into epoxy resin-reinforced carbon fibers, achieving a 50 % improvement in mode I energy fracture (G_{IC}). The architecture proposed by the authors promoted toughening through mechanisms such as CNT-nano bridging and carbon fiber extrinsic bridging. Similarly, Shin et al. [8] investigated the effect of varying CNT concentrations (ranging from 1 wt% to 9 wt%) on the interlaminar fracture toughness under mode II for epoxy/carbon fiber composites. The authors found an improvement of approximately 126 % when 3 wt% and 5 wt% CNTs were incorporated into the composite system. Additionally, the fracture surface revealed a rougher pattern, attributable to the bridging effect of the CNT, which requires more energy/load for crack initiation and propagation.

Carbon nanotubes promote interaction and adhesion between composite components, as investigated by Shanmugam et al. [19]. In their study, composites were prepared using methyl methacrylate (MMA) reinforced with ultra-high-molecular-weight polyethylene (UHMWPE) fibers. By applying a surface treatment to the fibers through a simple deposition of polydopamine (PA) containing 0.03 wt% of multi-walled carbon nanotubes (MWCNT), they achieved a 42.5 % improvement in mode I interlaminar fracture toughness. Similarly, carbon nanofibers (CNF) have demonstrated the potential to increase interlaminar strength, as evidenced by Arai et al. [20]. In their research, CNFs were incorporated in epoxy/carbon fiber composites, and the effect was assessed under both quasi-static and dynamic conditions. Under quasi-static conditions, CNFs produced by CNT MWCNT-7 type induced an approximately 200 % increase in fracture toughness compared to the baseline laminate during the initial stage. Additionally, this property increased three times over the baseline laminate in the stable crack propagation region. Under dynamic loading, CNFs also shifted the number of cycles to failure by a minimum factor of 1.5, increasing fracture toughness by approximately 300 %.

As reported in the literature, carbon nanotube buckypapers improve the interlaminar fracture toughness of thermoset composites, both in mode I and II. The improvements are attributed to the CNT-bridging effect which generally required more energy for crack growth. However, studies on three-phase composites (matrix, fiber and nanoparticles) particularly those composed of high-performance thermoplastic, have not been properly explored. In this context, the current work has as its main contribution to evaluate the contribution of buckypaper layers on mode I and II fatigue delamination of poly (ether imide) (PEI) and poly (aryl ether ketone) (PAEK) thermoplastic composites. Also, the fatigue data has been investigated through a physics-based approach to elucidate delamination growth, allowing a more precise correlation between fatigue data and the underlying micro-mechanisms. It is crucial to note that three-phase structural composites, particularly those comprising high-performance thermoplastics, remain underexplored in the existing literature. Consequently, with the advancement in using buckypapers to enhance multifunctionality, a comprehensive understanding of the fatigue properties of these materials is imperative.

2. Experimental procedures

2.1. Materials

Carbon nanotube buckypapers were fabricated using multi-walled carbon nanotubes (MWCNT) functionalized with a carboxyl group (COOH), supplied by the German company Nanografi. The MWCNTs exhibited internal and external diameters of 5–10 nm and 8–15 nm, respectively, with lengths varying from 1 to 3 μm. A polymeric mat was produced through electrospinning of PEI solution dissolved in N-methyl-2-pyrrolidone/dimethylacetamide (NMP/DMAC) in a 7:3 vol ratio. Both solvents were provided by Neon Commercial (a Brazilian company that commercializes different types of solvents), and PEI by Sabic's Innovative Plastics (a Saudi Arabian company that supplies polymers), in pellets form, under commercial name ULTEM 1000. Triton X-100, a surfactant supplied by Neon Commercial, was utilized for the non-covalent functionalization of the MWCNTs. Laminates were manufactured using TC1225 (PAEK/carbon) and TC1000 Premium (PEI/carbon fiber) semipregs, both supplied by Toray Advanced Composites (TAC) (the fabric located in Netherlands responsible for producing these semipregs).

2.2. Buckypaper fabrication

The fabrication of buckypapers was conducted via a vacuum filtration technique, following process parameters established in prior studies [4,21]. Briefly, a suspension composed of carbon nanotubes, deionized water, and Triton X-100 was sonicated using a Hielscherultrasonic tip (model UP400st), manufactured by a German company specializing in high-performance equipment. The resulting suspension underwent centrifugation, followed by vacuum filtration using a custom-built apparatus. The filtration setup incorporated a nylon membrane (porosity of 0.45 μm) and two layers of electrospun PEI mats. After the complete filtration of the suspension, the buckypapers were dried in a vacuum oven for 8 h at 100 °C.

2.3. Composite processing and sample preparation

The manufacturing process involved stacking 16 semipreg layers of PEI and PAEK semipregs, each reinforced with carbon fibers, to form laminates. The BP was strategically positioned at the mid-plane of the laminate, i.e., after the eighth layer. A polyimide film with a thickness of 0.13 μm was inserted to induce a pre-crack, as recommended by mechanical testing standards. The laminates were consolidated using a hydraulic press with heating and cooling controls. The processing parameters of PEI composites were heating up to 350 °C, followed by a 30-

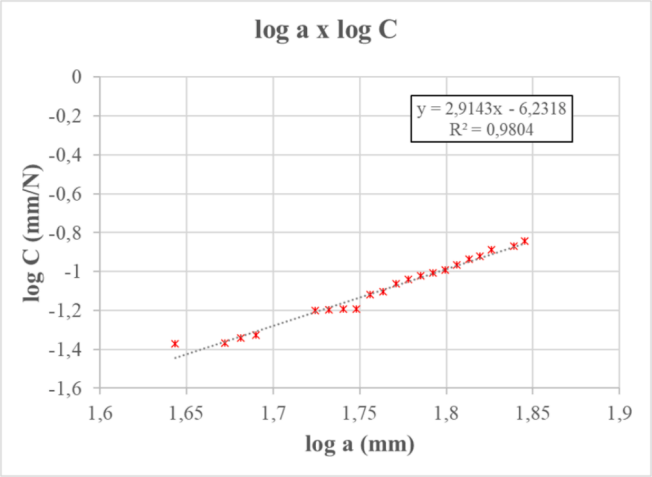

Fig. 1. Example of the curve a (crack length) versus C (compliance).

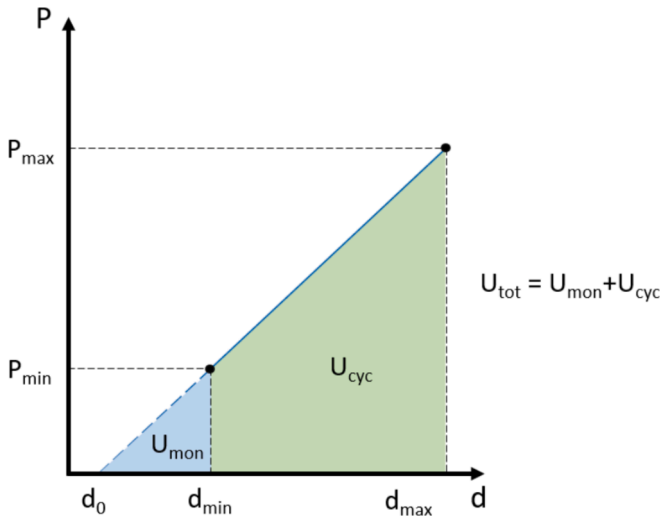

Fig. 2. Representative scheme of load versus displacement for a fatigue test on a linear elastic material (under displacement control). This scheme was adapted from Pascoe [20].

minute plateau for temperature homogenization. Subsequently, a pressure of 2 MPa was applied and maintained until the end of the cycle. After 20 min, the laminate was cooled to room temperature. The PAEK laminates were processed under identical conditions, except for a reduced pressure of 1 MPa. Composites with dimensions of (500 x 500 x 5) mm were fabricated and compared to buckypapers laminates, with a volumetric fraction of carbon nanotubes at 3.0 wt%.

Post-manufacturing, the samples were sectioned using a Proth cutting grinding machine equipped with a diamond disc. The dimensions of the samples were in agreement with ASTM D 5528 for the double cantilever beam (DCB) test and ASTM D7905 for the end-notched flexure (ENF) test. The DCB test specimens measured (165 × 25 × 5) mm, with a pre-crack length of 40 mm, while the ENF test specimens had similar dimensions but with a pre-crack length of 45 mm. For both types of samples, one side was sanded and painted with white paint to enhance crack visibility. Notably, for the DCB tests, an aluminum block was affixed to one end of each specimen.

2.4. Fatigue testing

Fatigue tests were conducted using a servo-hydraulic machine from MTS with a 10 kN load cell and a high-resolution camera to monitor the crack propagation. Before each test, samples were pre-cracked under mode-I or mode-II quasi-static loading to establish a crack tip. All experiments were performed under displacement control. As a result, the strain energy release and crack growth rates were initially elevated due to increasing crack length and damage, subsequently decreasing over time.

The DCB tests adhered to ASTM D6115-97 [22] and followed the test protocol outlined by Alderliesten and Brunner [23], employing a frequency of 5 Hz and a displacement ratio ($R_d = \delta_{min}/\delta_{max}$) of 0.1. Each specimen underwent multiple fatigue tests on the same sample to mitigate the fiber-bridging effect. Following the initial fatigue test, the obtained parameters (maximum displacement (δ_{max}) and the crack length) were recorded at the point that the pre-cracking of the test stopped, with the minimum displacement conforming to the displacement ratio of 0.1 and established upon loading from pre-cracking as stated in the protocol [23]. Specimens remained in the testing apparatus between successive fatigue tests. Data from mode-I fatigue tests were analyzed using the Paris' relationship, a fracture mechanics-based method widely applied in fatigue-induced delamination investigation, given by:

$$\frac{da}{dN} = C(\Delta\sqrt{G_i})^n = C[(\sqrt{G_{i,max}} - \sqrt{G_{i,min}})^2]^n \quad (2)$$

where C and n are curve fitting parameters, $G_{i,max}$ and $G_{i,min}$ are the maximum and minimum SERR (strain energy release rate) regarding the fatigue cycle, and i represents the mode I, when DCB test configuration is been carried on or mode II, for ENF test. The parameter C refers to compliance, which is the displacement (δ) divided by the load (P), parameter reported on ASTM standards. Therefore, for each data set, a graph of a (crack length) as a function of C is plotted, and the value of n (slope of the line) represents the angular coefficient of this line. One example of the graph a x C is presented on Fig. 1. The G_{max} and G_{min} were calculated according to the compliance calibration (CC) method as recommended by ASTM D5528-13, according to Equation (3). The da/dN values was obtained using the 7-point Increment Polynominal method.

$$G_{IC} = \frac{nP\delta}{2ba} \quad (3)$$

Where the exponent n is obtained from the slope of the graph a versus C ($compliance - \delta_i/P_i$), P is the load, δ is the displacement, b is the width, and a is the crack length.

The ENF testing procedure followed the methodology established by Amaral et al. [24] and O'Brien et al. [25], utilizing a testing frequency of 2 Hz, a displacement ratio of 0.1, and three samples of each material. The choice of a lower frequency was motivated by noise interference observed in displacement and load channels at elevated frequencies. The G_{IImax} derived from the pre-cracking process served as a benchmark for the fatigue test. Crack length during the test was accurately determined using the compliance calibration method. Additionally, for mode-II fatigue tests, a quantitative analysis of the data was conducted using the Paris' law relation (equation (4), and the calculation of the SERR for each fatigue cycle employed the classical beam–load deflection method (Equation (4).

$$G_{IIC} = \frac{9Pa^2\delta_d}{2B(2L^3 + 3a^3)} \quad (4)$$

where P is the load, a is the crack length, δ_d is the displacement, B is the sample width, and L is half of the span length.

The Paris relationship used to analyze the data from mode-I and mode-II tests represents a phenomenological approach, bridging the gap between macroscopic behavior and microscopic mechanisms. The strain energy released during the fatigue tests was computed following the methodology outlined by Pascoe [26]. This approach assumes that the linear elasticity is equivalent to the strain energy stored in the specimen. The monotonic energy (U_{mon}) corresponds to energy stored during the

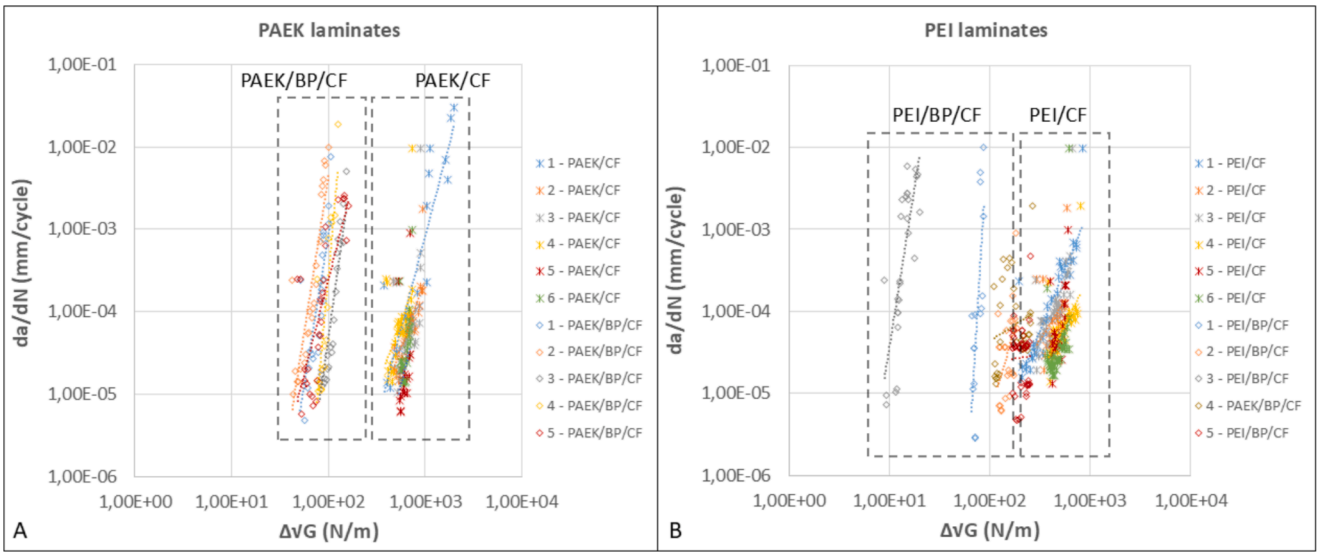

Fig. 3. – Fatigue resistance curves under mode-I for (a) PAEK and (b) PEI laminates. For both graphs, the stars and lozenge shapes represent the materials without and with buckypapers, respectively.

initial load cycles as the displacement increases from d_0 to d_{min}. Subsequently, additional energy is incorporated as the displacements increase from d_{min} to d_{max}. In the absence of energy dissipation, this energy is recovered by the loading apparatus during specimen unloading, commonly referred to as cyclic energy (U_{cyc}). Therefore, the system energy ($U_{tot} = U_{cyc} + U_{mono}$) remains constant throughout the fatigue test under displacement control and without energy dissipation. The methodology, schematically illustrated in Fig. 2, is grounded in energy balance principles, facilitating the correlation between macroscopic behavior and microscopic mechanisms.

During both fatigue tests (DCB and ENF), crack growth rates (da/dN) and energy dissipation rates (dU/dN) were calculated, with displacement and load, both minimum and maxiumu, values recorded for each cycle, with a camera system programmed to capture crack length data at specified intervals. They are each 100 cycles in the first 5,000 cycles, every 500 cycles from 5,000 to 15,000 cycles, every 1,000 cycles from 15,000 to 50,000, every 2,000 cycles from 50,000 to 100,000, and every 4,000 cycles from 100,000 to 500,000. The fatigue tests were terminated upon reaching a crack growth rate of 10^{-6} mm/cycle, defined as the point at which no crack propagation of 0.05 mm was observed in 200,000 cycles. It is important to highlight that all experiments were conducted under controlled conditions, maintaining a temperature of 21 °C and a humidity level of 55 %, respectively.

2.5. Fractographic analysis

Fracture surfaces generated under dynamic conditions (mode I and mode II) underwent morphology analysis using an optical microscope from Keyence, an American company, model VR-5000 wide-area 3D measuring system, and a scanning electron microscope from JEOL, a Japanese company, model JSM-840 EDS. Notably, no surface preparation was carried out prior to either analysis to prevent alterations to the surface characteristics. Optical microscopy was employed to quantitatively assess the surface roughness of the samples using the focus variation technique. This method involves capturing a series of images as the lens is displaced vertically, using the fracture surface as a reference, resulting in both in-focus and out-of-focus images. The microscope identifies and quantifies the in-focus pixels to build an entirely focused image. The depth of field for each plane and the generated focused image contribute to calculating the roughness via the arithmetical mean height (S_a), as per

$$S_a = \frac{1}{A}\int_A^n \int |Z(x,y)|dxdy \quad (5)$$

On the other hand, the main goal of SEM was to investigate the micromechanical mechanisms involved in crack propagation, as evidenced on the fracture surfaces. The analysis was conducted under the following conditions: a working distance of 10 mm and a probe current of 5 kV. In addition, a thin gold coating over the surface of the samples was necessary to ensure good electrical conductivity.

3. Results and discussion

3.1. Mode-I fatigue tests

One of the goals of this research is to evaluate the effect of buckypapers on the interlaminar fracture toughness of the thermoplastic composites submitted to dynamic conditions. Both laminate groups were submitted to five and six consecutive fatigue tests, respectively. Potential sources of variability can be mitigated by not removing the specimens from the testing apparatus. Following ASTM E647 and ASTM D5528-13, the fatigue data for mode-I testing were initially analyzed using Paris' law, where $\Delta\sqrt{G}$ is the similitude parameter. The SERR and the crack growth rates were calculated using the compliance calibration (CC) method and the 7-point Incremental Polynomial Method.

Fig. 3 shows the Paris curve for PAEK and PEI laminates submitted to fatigue tests under mode-I. The approach developed by Alderliesten and Brunner [23] consists of performing consecutive fatigue tests on the same specimen to assess the impact of the fiber bridging. As reported in the literature [23,27], increased fiber bridging results in enhanced strain energy storage and release cycle, elevating the SERR values and, consequently, shifting the curves to higher values. Here however, woven fabric was used as reinforcement, which was observed to exhibit fiber bridging only close to the crack tip. Hence, the bridging is not extensive enough to significantly alter the SERR values and to cause a notable shift in the curves. Also, the increase in the crack length does not substantially affect the extent of fiber bridging, resulting in similar values of $\Delta\sqrt{G}$ during the crack propagation. The absence of fiber bridging is consistent with observations from previous quasi-static tests, as there is no rising in the R-curve [4].

The buckypaper incorporation in the laminates reduced $\Delta\sqrt{G}$ values, shifting the fatigue resistance curves to the lowest values. A similar trend was observed in a quasi-static test, indicating that buckypapers reduced

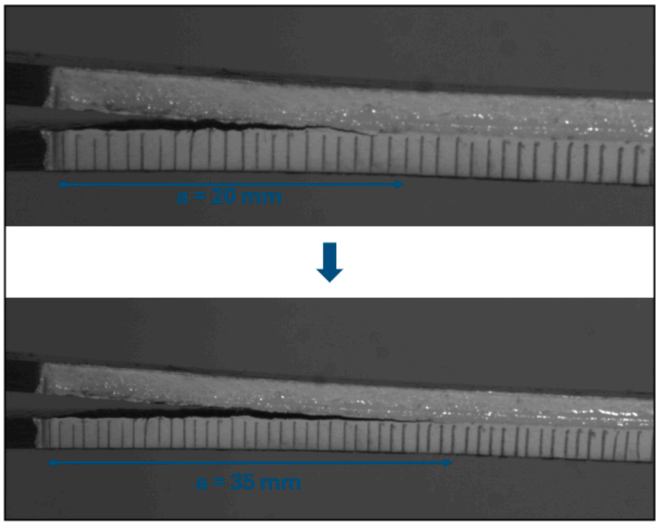

Fig. 4. – Observation of crack propagation during the second and third fatigue curves for PEI/BP/CF.

the interlaminar toughness of the composites [4]. This finding can be attributed to the pressure applied during compression molding, which favored the matrix to squeeze-out from the laminate. Consequently, only carbon nanotubes cohesively bonded by van der Wall forces remained as opposed to the robust covalent bonds typically present in the thermoplastic/CF interfacial region. PAEK/CB/CF composite exhibits a reduction of approximately one order of magnitude (Fig. 3a), whereas the decrease between PEI/CF and PEI/BP/CF laminates was less pronounced. In addition, the third fatigue curve for PEI/BP/CF (grey lozenges - Fig. 3b) presents the lowest values for this condition. This behavior is attributable to the crack tip stopping in the adjacent layer without buckypaper during the preceding test (second fatigue curve). During the crack opening procedure to ascertain the new δ_{max}, displacement and load were overestimated, leading to a crack growth of 15 mm when the crack returned to the layer containing buckypapers, as observed in Fig. 4. Consequently, a third added phase through the buckypaper layer shifted the curve to lower energy levels for both thermoplastics. It is noteworthy that the PEI thermoplastic displayed a greater scatter of results due to its high sensitivity in the layers where the crack propagated.

To further elucidate delamination phenomena, the physical concept of *G (-dU/dA)* during crack growth were employed to facilitate a more comprehensive correlation of the data. The total and the cyclic strain energy released due to crack growth are depicted in Fig. 5.

All buckypaper composites (represented by orange data points) are shifted to the lower energy levels and high exponents, indicating a reduced energy requirement for crack propagation. Additionally, there is higher dispersion in the fatigue data for laminates containing buckypapers, suggesting the heterogeneity of the results is related to the incorporation of the CNT film. For instance, PEI/BP/CF laminate demonstrates lower energy release and higher dispersion per unit area for BP composites. Consistent with the findings from quasi-static tests [4] buckypapers facilitate crack propagation, thereby reducing the interlaminar fracture toughness, the energy involved and, ultimately, the fatigue life of the composites. A similar trend is observed by analyzing the results of da/dN versus $\Delta\sqrt{G}$ data, albeit with reduced scatter. The behavior found in terms of U_{tot} and U_{cyc} curves is analogous, with the load ratio R = 0.1 and a reduced monotonic contribution.

This variability in the experimental points and the difference in the correlation coefficient are due to the application of the dU/dN fit to a set

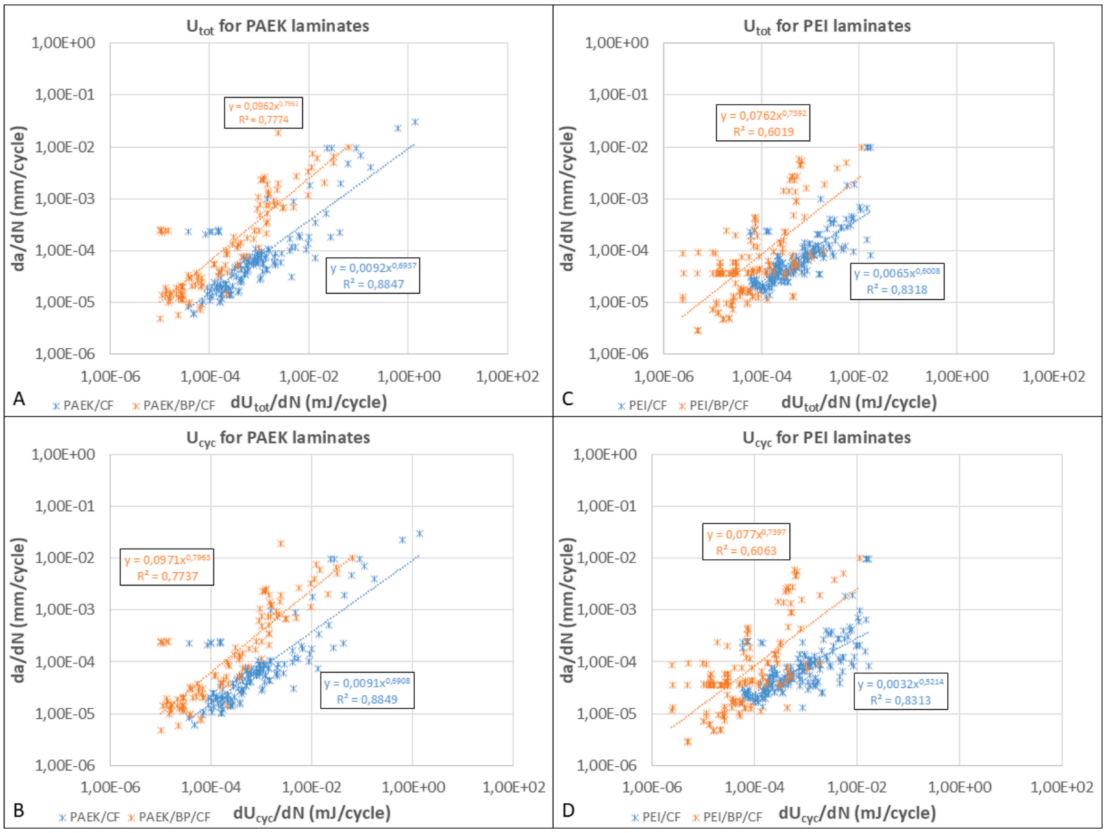

Fig. 5. – U_{tot} (total strain energy released) and U_{cyc} (cyclic strain energy released) during crack growth under mode-I loadings for PAEK e PEI laminates. Orange and blue data are for laminates with and without BP, respectively. (For interpretation of the references to colour in this figure legend, the reader is referred to the web version of this article.)

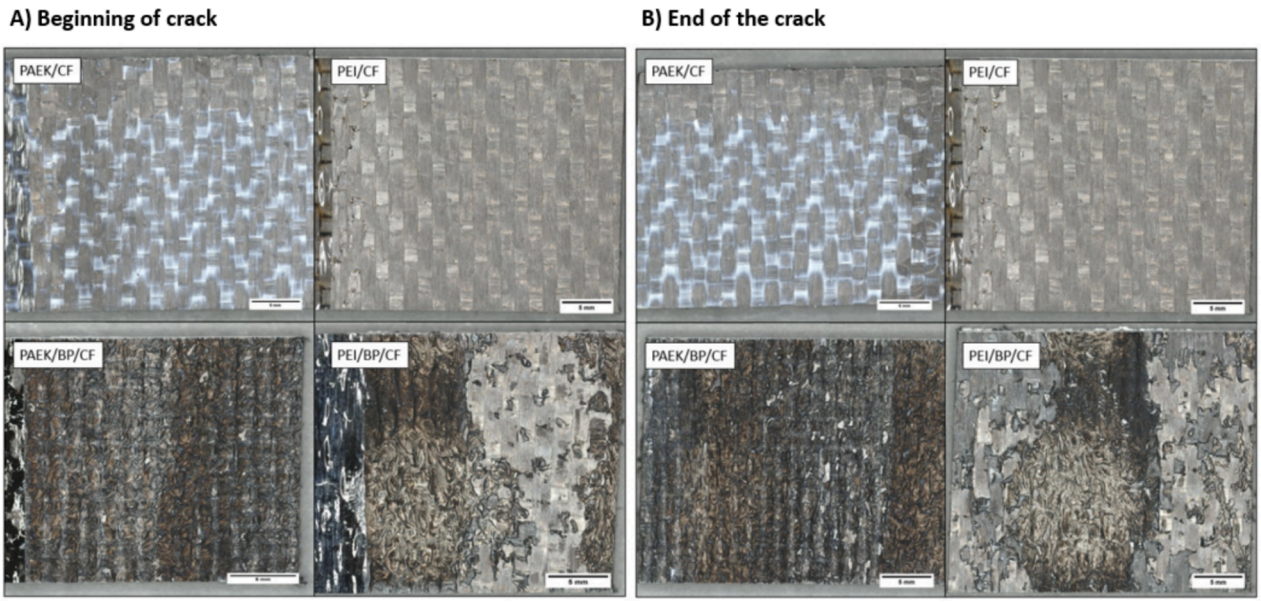

Fig. 6. – Micrographs obtained via optical microscopy for PAEK and PEI laminates at the beginning of the first fatigue curve.

Table 1
– Arithmetical mean height (Sa) for PAEK and PEI laminates at the beginning and end of the fracture surface relative to 1st fatigue curve.

Material	Arithmetical mean S_a (μm) Beginning	*Difference (%)	End	*Difference (%)	$\Delta_{B\text{-}E}$
PAEK/CF	59.276	–	66.934	–	7.658
PAEK/BP/CF	51.982	12.31	62.786	6.20	10.804
PEI/CF	106.017	–	131.885	–	25.887
PEI/BP/CF	71.906	32.17	83.570	36.63	11.664

* Reduction percentage of arithmetical mean Sa between laminate without and with BP.

of five samples using 7 points as a function to derive da/dN. Both factors preserve the variability observed during crack propagation and provide a more realistic representation of the relationship between the experimental data (da/dN versus dU/dN). In addition, the presence of a third phase (buckypapers) introduces variability into the crack propagation behaviour, as evidenced by the greater scatter observed in the orange curves. When comparing the behaviour of the materials, the PEI curve shows more dispersion than the PEAK curve. Analysis of the difference in R^2 between materials with and without buckypaper shows that PEI is more sensitive to the presence of bulk paper ($\Delta R^2 = 0.225$), resulting in greater variability and uncertainty compared to PEAK ($\Delta R^2 = 0.107$).

The divergences in the energy released during crack growth indicate distinct micro-mechanisms that contribute to energy dissipation throughout the tests. As documented in the literature [28], crack growth entails the formation of new surfaces, which requires additional energy.

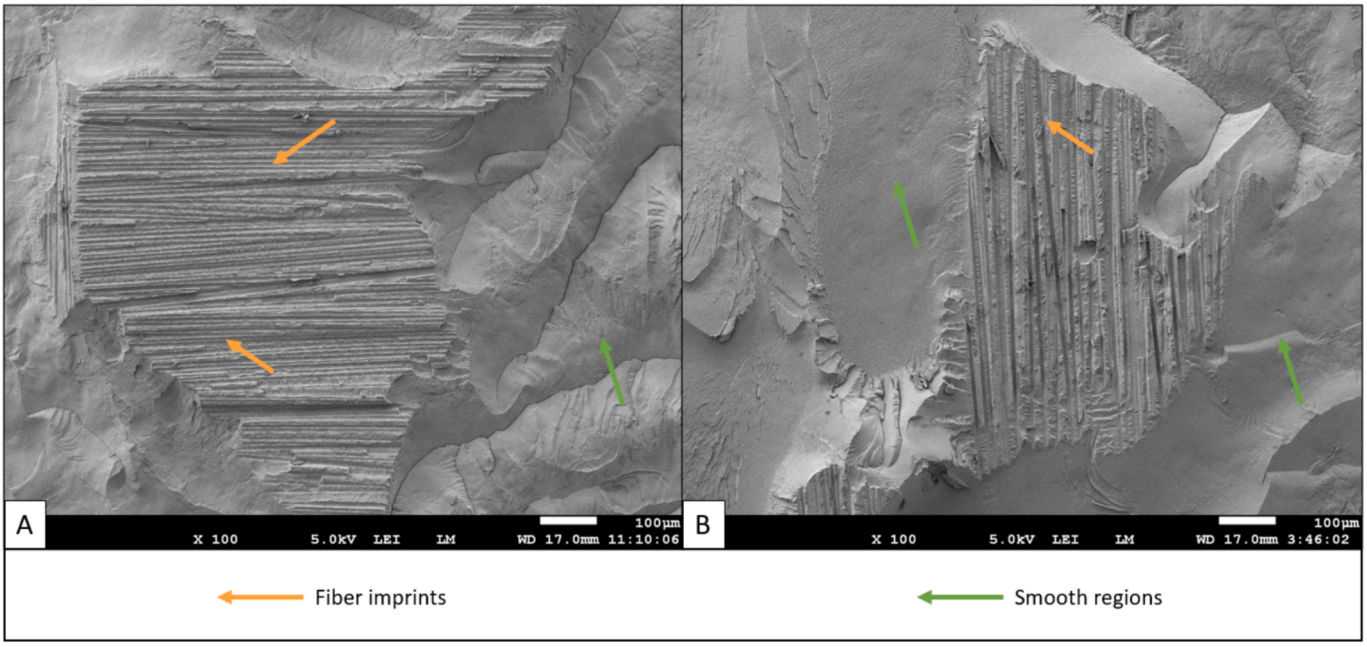

Fig. 7. – General view of the fracture surface obtained from mode-I fatigue tests for (a) PAEK/BP/CF and (b) PEI/BP/CF.

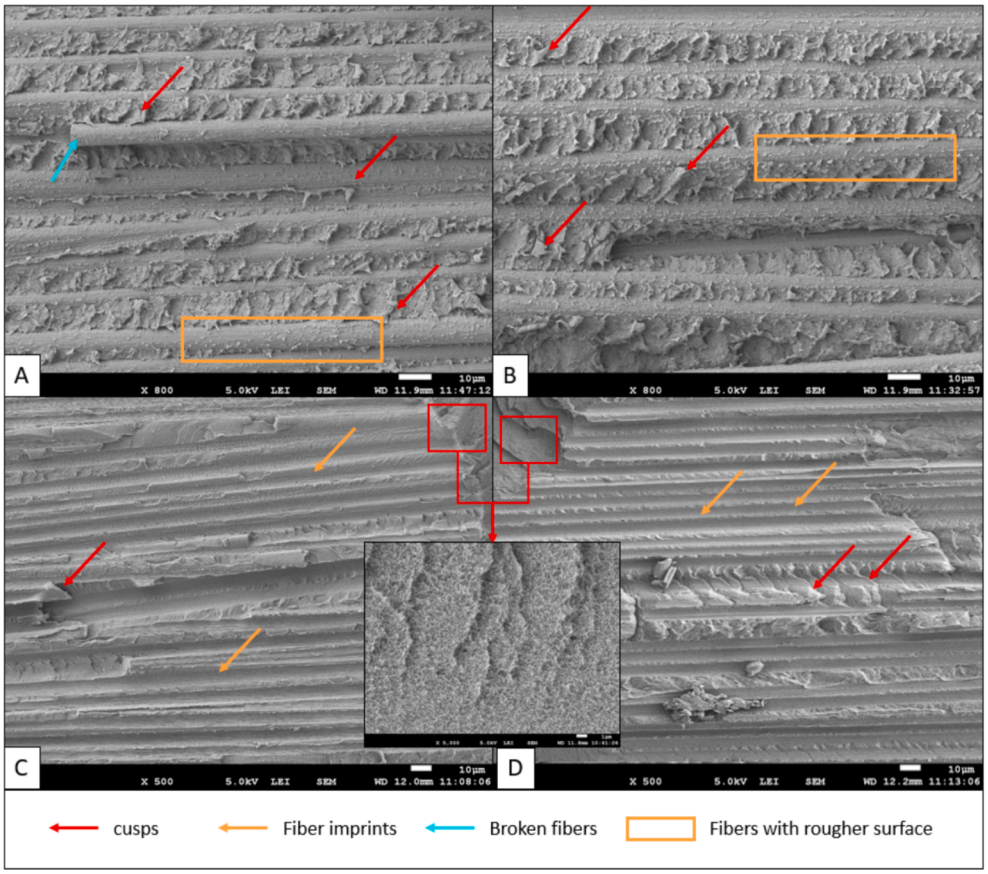

Fig. 8. – SEM micrograph of PAEK/CF (a)at the beginning and (b) at the end, and PAEK/BP/CF (c) at the beginning and (d) at the end of the crack growth.

Amaral [29] observed that the roughness pattern and micro-mechanisms of damage on the fracture surface are closely related to the energy released during crack propagation. Fig. 6a and 6b, obtained using optical microscopy, illustrate the fracture surface at the onset and end of the first fatigue curve, as well as the change in fracture roughness $\Delta_{B\text{-}E}$ (initial - final roughness). The roughness was quantified using the arithmetical mean height method, and the corresponding data are presented in Table 1. Notably, the incorporation of buckypaper promoted the reduction of the arithmetical mean height, indirectly representing a decrease in the energy associated with crack propagation. It is also noteworthy that the roughness at the end of the fatigue curve is higher than at the beginning, indicating the formation of additional micro-mechanisms of failure, increasing the energy dissipation, as the crack reach the steady-state region. According to Yao et al. [30], the fracture surface is smooth at the beginning of the crack propagation, with no matrix debris, and fiber/matrix debonding is the primary failure mechanism. However, as crack growth increases, hackles (or cusps) become evident, making the fracture surface rougher than at the initial stages of crack propagation. The SEM analysis will further confirm the presence of these mechanisms.

Another significant aspect is the disparity in crack growth behavior between the interface and the interior of the buckypaper, as regions with and without buckypaper are visibly distinct. SEM images (Fig. 7) depict one region corresponding to fiber imprints and another region that appears very smooth (green arrows), suggesting reduced energy dissipation. These smooth areas indicate that crack propagation occurred primarily within the matrix. Consequently, these smooth regions were excluded during the SEM examination.

Figs. 8 and 9 display SEM micrographs of the fracture surface of PAEK and PEI laminates, respectively. PAEK laminates indicate the presence of buckypaper reduced the roughness of the surface. For PAEK/CF laminates (Fig. 8a and 8b), the predominant failure mechanisms include broken fibers (blue arrow), fibers with rougher surfaces (orange rectangles), and cusps (red arrows). These cusps are typical for mode-II fracture surfaces [30], although in this context, they may be attributed to fiber pull-out, which generates shear stresses in the surrounding matrix. The PAEK/BP/CF composite (Fig. 8c and 8d) exhibits low roughness, with its fracture surface primarily composed of fiber imprints, indicating that the interface is a weak path. Smooth regions (red squares) are also evident for PAEK/CF/BP, corresponding to dense areas of carbon nanotubes. As carbon nanotubes are bonded by van der Walls forces, their fracture surface appears smooth, as reported by Wu et al. [31]. A comparison of the fracture surface at the beginning (Fig. 8a and 8c) and at the end (Fig. 8b and 7d) of crack growth reveals an increase in failure mechanisms. Also, the end of crack propagation is characterized by higher roughness, an indicative of substantial energy dissipation.

The SEM analysis of PEI laminates shows a similar trend to that observed in PAEK composites, increasing from the beginning (Fig. 9a and 9c) to the end (Fig. 9b and 9d) of crack propagation. PEI/CF laminate also exhibits greater roughness than PEI/BP/CF composite, with features such as fiber imprints (orange arrows), matrix debris (red circles), cusps, and river lines (yellow arrows), which are associated with loads applied to the fracture surface during the opening of the specimen [30,32]. In contrast, the fracture mechanisms in the PEI/BP/CF material predominantly consist of fiber imprints, with only a few regions displaying cusps. Additionally, some smooth areas (red rectangles) may be attributed to the presence of carbon nanotubes.

3.2. *Mode-II fatigue tests*

The influence of buckypaper on the interlaminar fracture toughness under mode II was investigated using End-Notched Flexure (ENF) tests. This investigation employed three samples of each material for the fatigue experiments, as the methodology developed by Alderliesten and

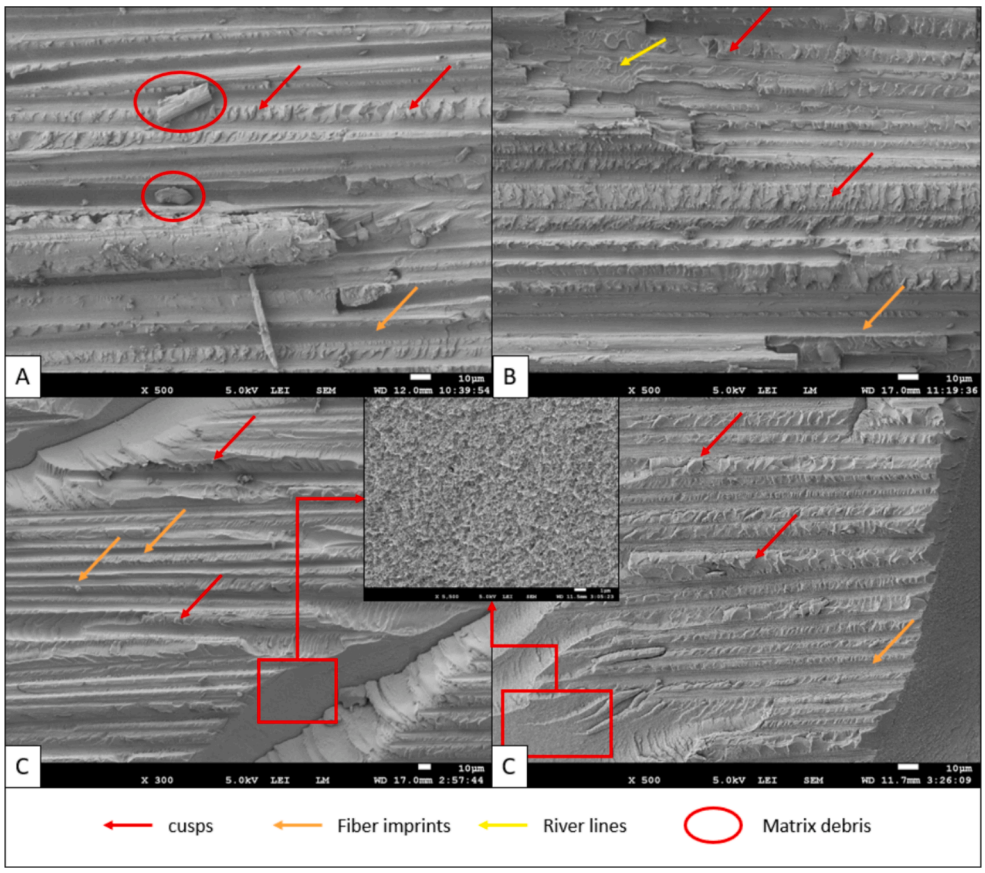

Fig. 9. – SEM micrograph of PEI/CF (a)at the beginning and (b) at the end, and PEI/BP/CF (c) at the beginning and (d) at the end of the crack growth.

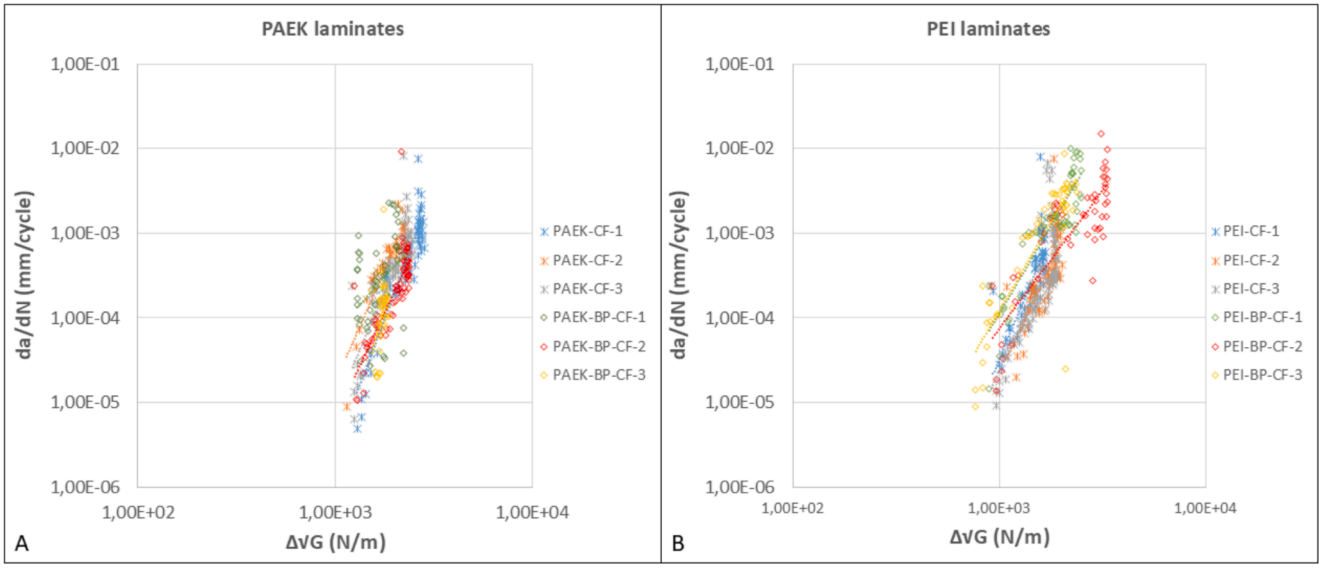

Fig. 10. – Fatigue resistance curves under mode-II for (a) PAEK and (b) PEI laminates. For both graphs, the stars and lozenge shapes represent the materials without and with buckypapers, respectively.

Brunner [23] was inapplicable due to a limited length to conduct multiple fatigue cycles, allowing for only a single fatigue curve per specimen. Following the recommendations of ASTM D7905-14 and Amaral et al. [24], the mode-II data were initially analyzed using the Paris relation, with $\Delta\sqrt{G}$ serving as the similitude parameter. The SERR during a fatigue cycle was calculated using the classical beam–load–deflection method, and the crack growth rate was determined using the 7-point Incremental Polynomial Method.

Initially, the fatigue data under mode-II were analyzed by plotting $\Delta\sqrt{G}$ against the crack growth rate, *da/dN*. The results for PAEK and PEI laminates are presented in Fig. 10a-b, respectively. The incorporation of buckypaper does not significantly alter the fatigue behavior, as the fatigue curves of the BP composites overlap with those of the base laminates. Notably, only samples PEI-BP-CF-1 and PEI-BP-CF-2 (Fig. 10b)

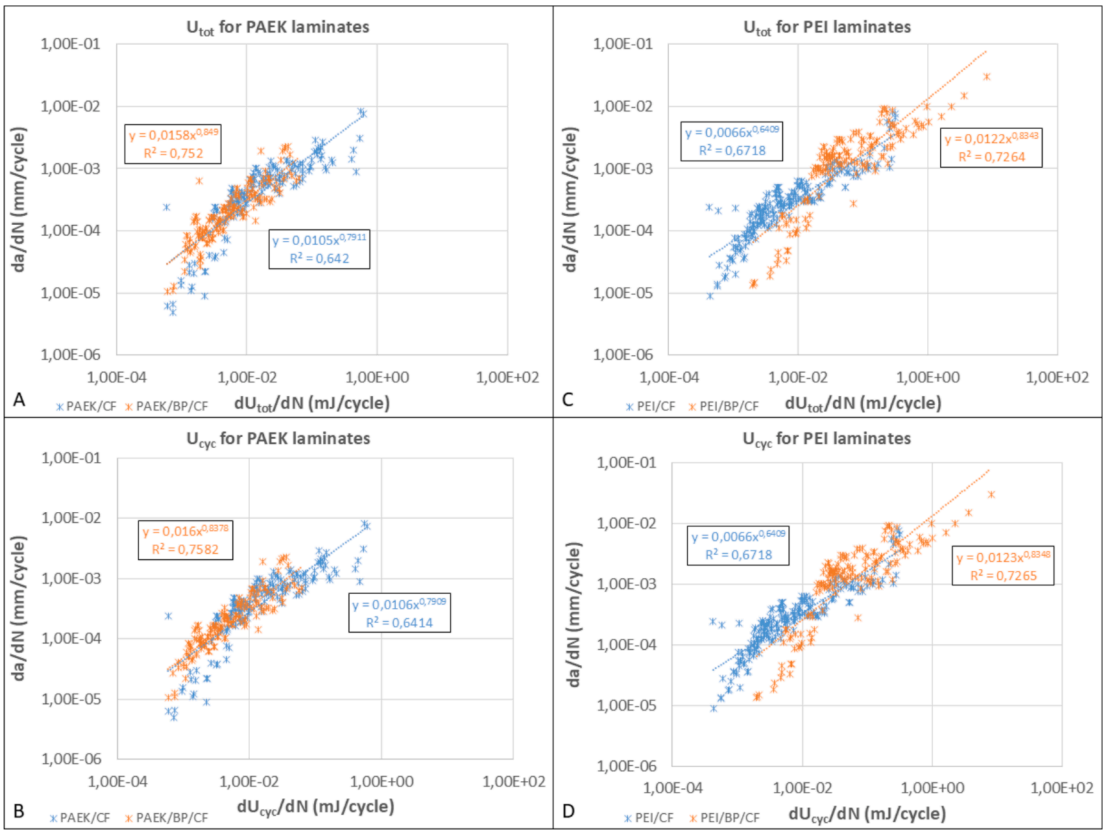

Fig. 11. – U_{tot} (total strain energy released) and U_{cyc} (cyclic strain energy released) during crack growth under mode II for PAEK and PEI laminates.

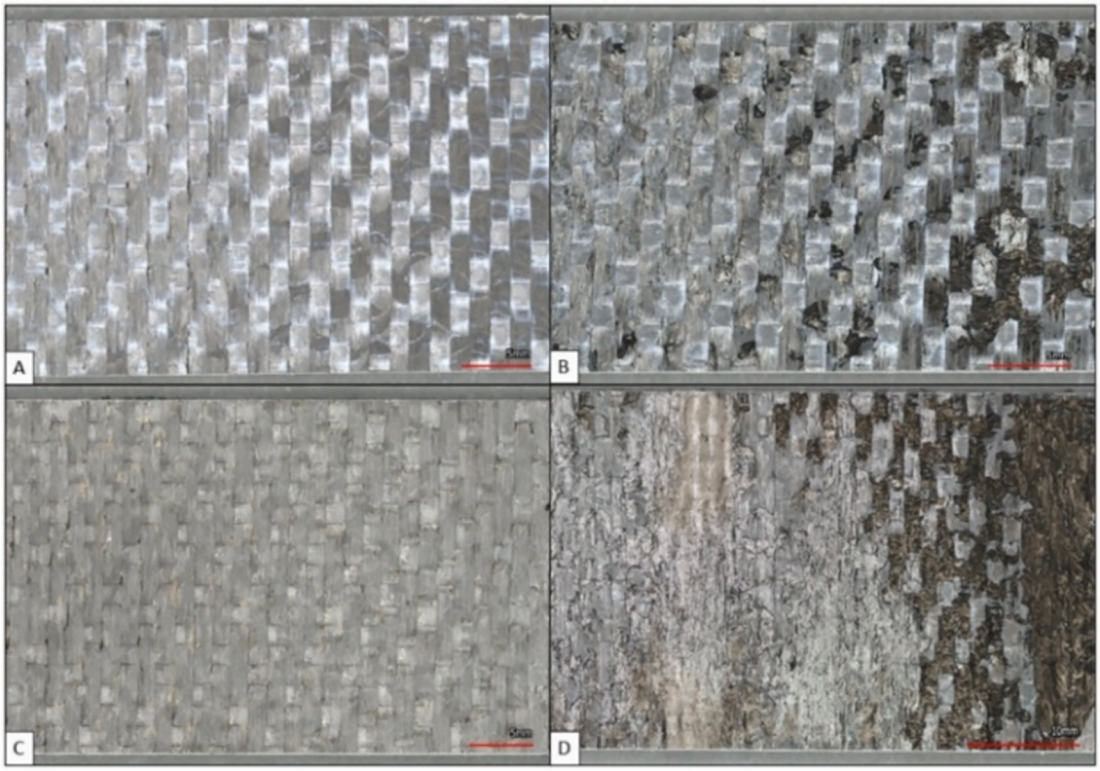

Fig. 12. – Optical micrographs of the fracture surfaces for (a) PAEK/CF, (b)PAEK/BP/CF, (c) PEI/CF, and (d) PEI/BP/CF.

Table 2
– Arithmetical mean height (Sa) of the fracture surfaces obtained under mode II fatigue tests for PAEK and PEI laminates.

Material	Arithmetical mean (S_a) (μm)	*Diference (%)
PAEK/CF	40.416	–
PAEK/BP/CF	54.231	34.18
PEI/CF	49.403	–
PEI/BP/CF	71.655	45.04

* Increase percentage of arithmetical mean (Sa) between laminate without and with BP.

exhibited higher $\Delta\sqrt{G}$ values at elevated crack growth rates, suggesting that carbon nanotubes acted as a bridging agent, thereby increasing the values of SERR [4,33]. These findings are consistent with those observed in quasi-static tests, which demonstrated only a marginal improvement of approximately 5 %.

In the Paris curve, crack propagation is divided into three distinct regions. The first region (threshold) represents the slow crack growth phase. The second region is characterised by linear crack propagation behaviour, where there is a linear relationship between (da/dN) and the strain energy release rate (SERR). It is in this region that the Paris fit is applied. Finally, the third region returns to non-linear behaviour, representing unstable crack propagation as it approaches the critical fracture value. In this study, the full curve was used as a reference for future modelling and design scenarios where it may be necessary to capture values near the threshold or critical fracture. However, the linearisation of the Paris curve was performed specifically in Region II using the linear portion of the experimental data points.

Fig. 11 illustrates the total and cyclic strain energy released due to crack growth. Considering the coefficient of determination (R^2), it is evident that BP composites (PAEK/BP/CF and PEI/BP/CF) display less scatter results compared to base laminates (PAEK/CF and PEI/CF). An additional factor that can be examined to enhance the understanding of fatigue delamination behavior under mode II is the correlation between the exponent (β) of the power trendline and resistance to delamination growth, where a higher β value indicates lower energy requirements for crack propagation [34]. PAEK/BP/CF and PEI/BP/CF laminates exhibited the highest β values, followed by PAEK/CF and PEI/CF composites, suggesting that less energy is required for shear damage and progression, which consequently results in a lower capacity for damage accumulation and extended fatigue life.

The dU/dN model evaluates the energy dissipation per cycle and as such does not show sensitivity to capture the non-linear behaviour inherent in regions I (threshold) and III (critical fracture). Consequently, this model is not suitable for determining parameters associated with these regions. As a result, the non-linearity observed in Fig. 10 is not evident in Fig. 11, highlighting the importance of using multiple models to gain a comprehensive understanding of crack propagation behaviour.

The principle of energy balance can be correlated with the micromechanisms involved in crack growth. As a result, rougher surfaces indicate increased damage propagation and the formation of damage features, which consume more energy per unit area [24,34]. Optical microscopy was initially performed to evaluate the roughness of the fracture surfaces, and the images are visualized in Fig. 12. The roughness values were compiled and are shown in Table 2. The roughness values exhibit the same trend observed in quasi-static tests and fatigue results reported so far. Accordingly, BP composites have a higher arithmetical mean (S_a) than the standard materials (without buckypapers). Thus, higher roughness implies more formation of damage features, also a higher effective fracture surface relative to the projected fracture plane, which increased energy involvement in crack propagation. Another observed characteristic is the presence of the buckypaper over the entire

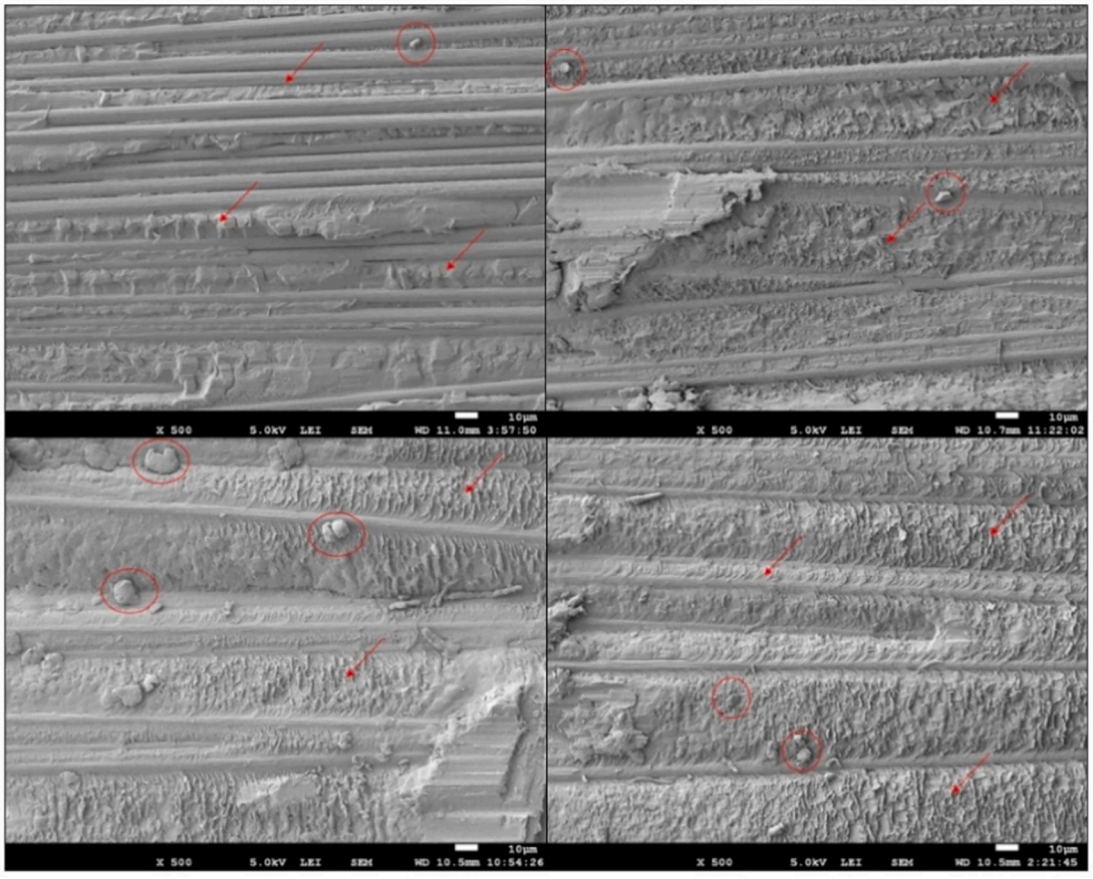

Fig. 13. – SEM micrographs of the fracture surfaces under mode-II for (a) PAEK/CF, (b) PAEK/BP/CF, (c) PEI/CF, and (d) PEI/BP/CF composites.

crack length, with its content increasing along the crack length.

The crack growth under mode II tends to create angular damage features in front of the crack tip, which propagates through the coalescence of these features, generating cusp-like structures. The quasi-static tests also reported this behavior [4]. The SEM images for PAEK and PEI laminates are presented in Fig. 13. As noted, all surfaces display a similar fracture pattern, primarily composed of cusps and matrix debris over the crack length. It is worth mentioning that both aspects are related to friction between the surfaces during the shear loading, as also observed by Amaral et al. [24] and Monticeli et al. [34]. The cusps appeared as inclined platelets on the surface. Also, their distribution and size can be influenced by the processing conditions, the spacing between the fibers, the temperature, the moisture, and the matrix toughness [30]. Consequently, the buckypaper acted as a bridge, enhancing the toughness of the interlaminar region, which led to an increase in cusp thickness. The higher content of cusps for PAEK/BP/CF (Fig. 13b) and PEI/BP/CF (Fig. 13d) also indicates that more energy was expended to generate such features.

Summarizing, the incorporation of carbon nanotube buckypapers as interlayer differently affected the interlaminar fracture toughness of the three-phase composites produced, where, on the one hand, BP can reduce the composite resistance to crack growth on mode I, where it acted as an easy pathway to crack growth. However, it also increases the interlaminar fracture toughness through the bridging effect of the carbon nanotubes. This study brings the necessity to stop only testing one mode and then claim success if the other mode has not been presented and obtained success to support the findings. This proper investigation would provide a deeper understanding of delamination mechanisms and help optimize composite designs for improved interlaminar performance.

4. Conclusions

This work investigates the influence of carbon nanotube buckypapers on fatigue crack propagation under individual modes I and II applied for PEI- and PAEK-based matrix composites. For this purpose, three-phase composites (matrix, carbon fiber and nanoparticles) were produced via hot compression molding and then submitted to a fatigue test to understand how buckypapers affect fracture toughness under dynamic conditions. The phenomenological and physical approaches employed helped to understand the fracture toughness of composites reinforced with buckypapers. In addition, the fractographic study contributes to understanding the mechanisms involved in crack propagation and how the crack propagates in each opening mode. The main findings drawn from this experimental article are as follows:

- The incorporation of buckypapers reduces interlaminar fracture toughness in mode-I for both, PAEK/BP/CF and PEI/BP/CF composites. Consistent with previous findings, buckypapers create a preferential crack path, promoting growth and reducing fatigue delamination resistance by an order of magnitude.
- Conversely, the inclusion of buckypaper alters the fatigue behaviour of the composites in mode II, where PEI/BP/CF shifts for higher $\Delta\sqrt{G}$, suggesting that carbon nanotubes acted as a bridging agent, increasing the SERR. Consequently, these composites exhibit increased damage accumulation capacity, extended fatigue life and improved resistance to shear fatigue delamination.
- Fractographic analysis revealed that smooth specimen surfaces with minimal evidence of matrix and bulb failure were more prone to Mode I. On the other hand, composites subjected to Mode II showed rougher fracture surfaces with more pronounced damage for both PAEK and PEI/BP composites, consistent with the bridging effect of the carbon nanotubes favoring the increase in SERR.

CRediT authorship contribution statement

Luis Felipe de Paula Santos: Writing – original draft, Methodology, Investigation, Data curation, Conceptualization. **Francisco Maciel Monticeli:** Writing – review & editing, Writing – original draft, Formal analysis, Conceptualization. **Bruno Ribeiro:** Writing – review & editing, Methodology, Investigation, Conceptualization. **Michelle Leali Costa:** Writing – review & editing, Supervision, Funding acquisition. **René Alderliesten:** Writing – review & editing, Supervision, Methodology, Formal analysis. **Edson Cocchieri Botelho:** Writing – review & editing, Supervision, Funding acquisition.

Declaration of competing interest

The authors declare that they have no known competing financial interests or personal relationships that could have appeared to influence the work reported in this paper.

Acknowledgments

The authors are grateful for the financial support given by the Brazilian Funding Institutions: São Paulo Foundation Research (FAPESP) (2018/07867-3 and 2019/18691-6), National Council for Scientific and Technological Development (CNPq) (140852/2018-2, 306576/2020-1 and 304876/2020-8) and this study was financed in part by the Coordenação de Aperfeiçoamento de Pessoal de Nível Superior – Brasil (CAPES) – Finance Code 001.

Data availability

The authors do not have permission to share data.

References

[1] Bhudolia SK, Gohel G, Vasudevan D, Leong KF, Gerard P. Delamination behaviour and surface morphology of wholly thermoplastic composites using different ultra-high molecular weight thermoplastic fabrics with pristine and toughened Elium resin under Mode I loading. Compos A Appl Sci Manuf 2023;164:107273. https://doi.org/10.1016/j.compositesa.2022.107273.
[2] Barbosa LCM, Souza SDBD, Botelho EC, Candido GM, Rezende MC. Fractographic study of welded joints of carbon fiber/PPS composites tested in lap shear. Eng Fail Anal 2018;93:172–82. https://doi.org/10.1016/j.engfailanal.2018.07.007.
[3] Faria MCMD, Appezzato FC, Costa ML, Oliveira PCD, Botelho EC. The effect of the ocean water immersion and UV ageing on the dynamic mechanical properties of the PPS/glass fiber composites. J Reinf Plast Compos 2011;30(20):1729–37. https://doi.org/10.1177/0731684411427483.
[4] de Paula Santos LF, Monticeli FM, Ribeiro B, Costa ML, Alderliesten R, Botelho EC. Does carbon nanotube buckypaper affect mode-I and II interlaminar fracture toughness under quasi-static loading? Compos Struct 2023;323. https://doi.org/10.1016/j.compstruct.2023.117507.
[5] Dikshit V, Bhudolia S, Joshi S. Multiscale polymer composites: A review of the interlaminar fracture toughness improvement. Fibers 2017;5:38. https://doi.org/10.3390/fib5040038.
[6] Donadon MV, de Almeida SFM. Damage modeling in composite structures. In Comprehensive Materials Processing: Elsevier; 2014. p. 111–47.
[7] Brunner AJ, Stelzer S, Pinter G, Terrasi GP. Mode II fatigue delamination resistance of advanced fiber-reinforced polymer–matrix laminates: Towards the development of a standardized test procedure. Int J Fatigue 2013;50:57–62. https://doi.org/10.1016/j.ijfatigue.2012.02.021.
[8] Leciñana I, Renart J, Turon A, Zurbitu J, Tijs BHAH. Characterization and analysis of the mode I interlaminar fatigue behaviour of thermoplastic composites considering R-curve effects. Eng Fract Mech 2023;286. https://doi.org/10.1016/j.engfracmech.2023.109273.
[9] Vinciquerra AJ, Davidson BD, Schaff JR, Smith SL. Determination of the mode II fatigue delamination toughness of laminated composites. J Reinf Plast Compos 2002;21:663–77. https://doi.org/10.1177/0731684402021007473.
[10] Amaral L, Yao L, Alderliesten R, Benedictus R. The relation between the strain energy release in fatigue and quasi-static crack growth. Eng Fract Mech 2015;145:86–97. https://doi.org/10.1016/j.engfracmech.2015.07.018.
[11] Jen YM, Huang YC. Improvement in tensile quasi-static and fatigue properties of carbon fiber-reinforced epoxy laminates with matrices modified by carbon nanotubes and graphene nanoplatelets hybrid nanofillers. Nanomaterials 2021;11. https://doi.org/10.3390/nano11123459.
[12] He Y, Duan K, Yao L, Tang J, Zhang J, Jiang D, et al. Synergistic toughening on CFRP via in-depth stitched CNTs. Compos B Eng 2023;254:110605. https://doi.org/10.1016/j.compositesb.2023.110605.

[13] Chung DDL. A review of multifunctional polymer-matrix structural composites. Compos B Eng 2019;160:644–60. https://doi.org/10.1016/j.compositesb.2018.12.117.
[14] Shin YC, Lee W, Kim Il. H. S.: Mode II interlaminar fracture toughness of carbon nanotubes/epoxy film-interleaved carbon fiber composites. Compos Struct 2020; 236:111808. https://doi.org/10.1016/j.compstruct.2019.111808.
[15] Shanmugam L, Kazemi ME, Rao Z, Lu D, Wang X, Wang B, et al. Enhanced Mode I fracture toughness of UHMWPE fabric/thermoplastic laminates with combined surface treatments of polydopamine and functionalized carbon nanotubes. Compos B Eng 2019;178:107450. https://doi.org/10.1016/j.compositesb.2019.107450.
[16] Arai M, Hirokawa JI, Hanamura Y, Ito H, Hojo M, Quaresimin M. Characteristic of mode i fatigue crack propagation of CFRP laminates toughened with CNF interlayer. Compos B Eng 2014;65:26–33. https://doi.org/10.1016/j.compositesb.2014.02.025.
[17] Santos, L. F. de P.; Alderliesen, R.; Kok, W.; Ribeiro, B.; Bovi, J. de O.; Costa, M. L.; Botelho, E. C.: The influence of carbon nanotube buckypaper / poly (ether imide) mats on the thermal properties of poly (ether imide) and poly (aryl ether ketone)/ carbon fiber laminates. **116** (2021). http://doi:10.1016/j.diamond.2021.108421.
[18] ASTM D 6115 – 97: Standard Test Method for Mode I Fatigue Delamination Growth Onset of Unidirectional. American Society for Testing and Materials (ASTM), **97**, 1–6 (2005). http://doi:10.1520/D6115-97R19.2.
[19] Alderliesten R, Brunner AJ. Determination of mode I fatigue delamination propagation in unidirectional fibre-reinforced polymer composites - E. ESIS TC 4 Test Protocol 2019;1:1–14.
[20] Amaral L, Zarouchas D, Alderliesten R, Benedictus R. Energy dissipation in mode II fatigue crack growth. Eng Fract Mech 2017;173:41–54. https://doi.org/10.1016/j.engfracmech.2017.01.020.
[21] O'Brien, T. K.; Johnston, W. M.; Toland, G. J.: Mode II Interlaminar Fracture Toughness and Fatigue Characterization of a Graphite Epoxy Composite Material. Nasa/Tm–2010-216838, , 1–32 (2010).
[22] Pascoe, J.-A.: Characterisation of Fatigue Crack Growth in Adhesive Bonds.
[23] Yao L, Cui H, Sun Y, Guo L, Chen X, Zhao M, et al. Fibre-bridged fatigue delamination in multidirectional composite laminates. Compos A Appl Sci Manuf 2018;115:175–86. https://doi.org/10.1016/j.compositesa.2018.09.027.
[24] Griffith A, A.: vi.. The phenomena of rupture and flow in solids. Philosophical transactions of the royal society of london. Series A, Containing Papers of a Mathematical or Phys. Character 1921;221:163–98. https://doi.org/10.1098/rsta.1921.0006.
[25] Greenhalgh ES. Delamination-dominated failures in polymer composites. In Failure Analysis and Fractography of Polymer Composites: Elsevier; 2009. p. 164–237.
[26] Wu Y, Cheng X, Chen S, Qu B, Wang R, Zhuo D, et al. In situ formation of a carbon nanotube buckypaper for improving the interlaminar properties of carbon fiber composites. Mater Des 2021;202. https://doi.org/10.1016/j.matdes.2021.109535.
[27] Santos LFP, Ribeiro B, Hein LRO, Alderliesten R, Zarouchas D, Botelho EC, et al. The effect of temperature on fatigue strength of poly(ether-imide)/multiwalled carbon nanotube/carbon fibers composites for aeronautical application. J Appl Polym Sci 2020;137:49160. https://doi.org/10.1002/app.49160.
[28] Li, N.; Wang, G. dong; Melly, S. K.; Peng, T.; Li, Y. C.; Di Zhao, Q.; de Ji, S.: Interlaminar properties of GFRP laminates toughened by CNTs buckypaper interlayer. Composite Structures, **208**, 13–22 (2019). http://doi:10.1016/j.compstruct.2018.10.002.
[29] Monticeli FM, Odila Hilario Cioffi M. Jacobus Cornelis Voorwald, H.: Mode II delamination of carbon-glass fiber/epoxy hybrid composite under fatigue loading. Int J Fatigue 2021;154:106574. https://doi.org/10.1016/j.ijfatigue.2021.106574.